CrystEngComm

ROYAL SOCIETY OF CHEMISTRY

PAPER

View Article Online
View Journal

Cite this: DOI: 10.1039/d6ce00102e

Directionality in cation–anion interactions involving chalconium cations

Mariusz Michalczyk, *[a] Steve Scheiner [b] and Wiktor Zierkiewicz *[a]

Received 4th February 2026,
Accepted 5th May 2026

DOI: 10.1039/d6ce00102e

rsc.li/crystengcomm

The directionality of bonds is an important feature for many compounds relevant in biochemistry, crystal engineering and materials chemistry. It is widely accepted that a good number of contacts between ions (including ionic bonds) are nondirectional. A CSD survey is employed to demonstrate that significant directionality of cation···anion interactions is observed for systems which include a chalconium cation. Nearly 70% of all found structures contain a R–Y···LB angle (Y = S, Se, Te; LB = atom from anionic Lewis base) within 10° of linearity. Such structural motifs are commonly termed charge-assisted chalcogen bonds. Quantum chemical analysis traces this angular tendency to a compromise between coulombic forces and exchange repulsion, which pull in opposite directions. Charge transfer, polarization, and dispersion terms are much smaller in magnitude and thus exert a lesser influence.

Introduction

It would be difficult to envisage chemistry without the concept of directionality in the noncovalent bonding between molecules. When considering hydrogen bonding in DNA or biologically relevant molecular recognition mechanisms, this essential phenomenon serves as the foundation of life.[1] The self-organization of assemblies observed in numerous crystal engineering and material chemistry studies[2–21] results from directionality primarily facilitated by relatively weak, reversible noncovalent interactions, notably including σ-hole interactions[22–24] alongside hydrogen bonds. Previous studies have shown that σ-hole interactions between neutral molecules can regulate the structuring of crystal geometries.[25,26] Very recently, directionality has been identified in the group of clusters stabilized by spodium bonds, a new class of σ-hole interactions.[18]

The clustering together of cations with anions is the basis of the concept of the ionic bond. When these ions are monoatomic, *e.g.* Na^+ or Cl^-, it is clear that their interactions will be isotropic. But there is some question as to whether the degree of anisotropy might be rather small even for certain polytatomic species such as NH_4^+,[27,28] or OH_3^+ (ref. 29) or in some cases a linear structure such as CN^-.[30] Indeed there is some thought in the literature that ionic bonds between cations and anions lack a high degree of directionality in the general case.[31,32] A recent article[33] claimed that "the lack of the dependence of the electrostatic attraction on the relative orientation of the cation and the anion results in the structural flexibility of ionic bonds… As a result, ionic bonds are of limited use for directional connectivity". On the other hand, there are multiple cases where the relative orientation of ions is readily understandable on the basis of certain chemical phenomena. Hutskalov *et al.*[33] observed ionic bond which was predictable in terms of directional orientation, in the pairing between *N*-methylpyridinium cations and arylsulfonate anions. The authors attributed the directionality to the presence of nonpolar hydrocarbon shields which wrapped the charged sites, leaving them the possibility to interact only in specific spatial direction. The 10 new structures obtained in this way were characterized by X-ray diffraction, 2D NMR ROESY experiment as well as computational protocols.[33] Another example of directional ionic bonds derives from a paper by Kong *et al.*[34] where the dipole-induced orientation of the ions produced linear calcium carbonate chains $(Ca^{2+}CO_3^{2-})_n$. The capping agent, triethylamine, was used to control the directional organization of the polymer (with up to 250 units).[34] In addition to these two unique ways for imparting directionality, organized self-assembling of ion-involved structures can be achieved by adding a group of other interactions,[35,36] introducing metal coordination,[37] in planar systems with unsaturated π-bonds[38] or in the ionic liquids.[39–42] Various crystal structures provide other examples of directional cation–anion interactions.[43–49]

Considering the enormous implications of directionality for the design of supramolecular architectures, coupled with the proliferation of systems that contain both cations and

[a] *Faculty of Chemistry, Wrocław University of Science and Technology, Wybrzeże Wyspiańskiego 27, 50-370 Wrocław, Poland.*
E-mail: mariusz.michalczyk@pwr.edu.pl, wiktor.zierkiewicz@pwr.edu.pl
[b] *Department of Chemistry and Biochemistry, Utah State University Logan, Utah 84322-0300, USA*

anions, the question of the role played by directionality in ion pairs takes on especial importance. As a particular area of focus, the chalcogen bond (ChB) has seen rapidly growing interest in recent years.[50–58] This noncovalent bond employs a S, Se, or Te atom as electron acceptor Y in combination with a Lewis base (LB) donor. Like its closely related H-bond cousin, the bonding is derived in large measure from a coulombic attraction, which is in turn due to the development of a positive region of electrostatic potential on the Y atom commonly known as a σ-hole. This attraction is supplemented by a certain amount of charge transfer from the LB into the σ*(YR) antibonding orbital of the acid. Since both the σ-hole and the aforementioned σ* orbital are concentrated in a small region of space, ChBs tend to be highly directional. The question arises as to whether their directionality persists when the chalcogen-containing Lewis acid takes on cationic character. And as a second factor, in connection with the considerations discussed above, what are the implications for this directionality if the electron-donor Lewis base is an anion, forming a chalcogen-bonded ion pair. The literature contains an awareness regarding the issue of the charge-assisted chalcogen bond (CAChB)[59–65] wherein the chalcogen bond is augmented by coexisting positive and negative charge on the monomers. It has been demonstrated that such quite strong interactions can be found in biochemical compounds[66–68] and can be effectively utilized in catalysis.[69]

As the research sample we chose the group of chalconium cations.[16,70,71] This sort of molecular ion (of +1 formal charge) comprises a hypervalent Y chalcogen atom (Y = S, Se, Te) bonded covalently with three R atoms (the same or different). An essential aspect of such a chalconium cation is that, despite the presence of a large positive molecular electrostatic potential (MEP) covering its entire surface, it contains specific locations of further decreased electron density on the extensions of the three R–Y covalent bonds. These strong MEP maxima can be interpreted as three σ-holes,[72,73] as their local value of MEP (labelled as $V_{S,max}$) is higher than the surroundings. Anisotropy in electron distribution is then evident in chalconium cations in similar fashion as typical, neutral σ-hole donors.[26,73–77] The consequence of the presence of three intense maxima of MEP at the chalconium cation is the enhanced capability to effectively bind Lewis bases. The directional bonding patterns between halonium cations and neutral HCN molecules acting as prototypical Lewis bases were examined in our recent investigation of the set of halonium cations that were the fragments of crystalline solids from the Cambridge Structural Database (CSD).[78] Effective acceptance of up to four hydrogen cyanides was confirmed therein. This strong acidic property was extensively studied for halonium, chalconium, and pniconium cations in the context of their application in organocatalysis[70,71,79,80] as the stabilizers of transition state structures, *e.g.* in the hydrolysis of methyl chloride,[70] addition of ammonia to acetone[70] or Schiff condensation between 4-methylbenzaldehyde and 2-aminopyridine.[71] It has been demonstrated that chalconium-based catalysts can be promising alternatives to metal-based Lewis acids.[79]

It is an intriguing question whether the existence of MEP maxima located on a chalconium cation is sufficient to guarantee the directionality of chalcogen bonds with an approaching anion. For the purposes of this work, the CSD was examined for the structural motif of the chalconium cations as well as the contacts made *via* the chalcogen bond between the chalcogen atom (S, Se, Te) and any ligand (neutral or ionic). Referring to actual structures from the CSD database improves the reliability of our study and the feasibility of applying our findings to generate other systems of precise 3D arrangement which can be exploited in supramolecular chemistry or organocatalysis.

Computational methods

Single-point calculations for geometries taken from crystal sources, as well as full optimization for model monomers of chalconium cations, were conducted using the M06-2X functional and the def2-tzvpp[81–84] basis set by means of the Gaussian 16 (Rev. D.01) code.[85] For direct theoretical evaluation, the cation-containing fragments of three crystal structures of reference codes: AMOLUM,[86] MEKCAI[87] and RILFOL[88] from the Cambridge Structural Database (CSD,[89] ver. 5.44 with all available updates, Conquest software ver. 2025.2.0) were selected. The optimized geometries of model cationic monomers were reviewed in terms of harmonic frequency analysis of normal modes which revealed no imaginary frequencies, confirming them as actual minima. The molecular electrostatic potential (MEP) analysis for all monomeric systems was performed utilizing the MultiWFN software (version 3.7)[90,91] to evaluate the MEP distribution and location of MEP maxima. Graphical layout was made using the VMD 1.9.4 (ref. 92) and Origin 2025 Pro software. The interaction energy for the dimers truncated from the crystal structures was calculated using the supermolecular approach. The basis set superposition error (BSSE) in the interaction energy calculations was removed *via* the counterpoise procedure.[93] Dissection of the interaction energy into its constituents was accomplished using the Head-Gordon ALMO-EDA scheme[94,95] and associated Q-Chem 6 package. LUMO orbital visualization was performed *via* Chemcraft software.[96]

CSD survey – directionality

As a first step, the CSD was surveyed to assess the frequency with which chalconium cations occur within the currently available crystallographic dataset. To this end, the following setup was designed in the Conquest software: we first set the chalcogen atom (Y = S, Se, Te) of assigned +1 charge, limited to be covalently bonded with any three atoms: *i.e.* $[R_3Y]^+$. All surveys used global criteria of structures with no errors, non-

disordered, with 3D coordinates determined and accuracy of crystal structure determination (*R* factor) with value lesser or equal to 0.1. It was found that the chalconium cation is a common feature, occurring in numerous deposited structures, more than 1100. The vast majority contained sulfur, some 844 systems, roughly 75% (see Fig. 1). Se and Te cations were retrieved less frequently, 119 and 168 times, respectively.

Such abundance of hits motivated us to perform the next step in CSD survey, namely searching for motifs of intermolecular contact between chalconium cation and any atom which was realized again by the Conquest program. The intermolecular contact was specified to be determined according to interatomic distances between Y and LB (LB = atom from neutral or ionic Lewis base) that are shorter than the sum of the van der Waals radii of given atoms. This condition is often considered as a first indicator of an attractive interaction. Additionally, for all contacts that satisfied these requirements, the R–Y···LB angles were recorded. This particular angle is crucial to ascertain the degree of directionality of Y···LB bonding in the surveyed structures. Values close to the perfect 180° indicate high directionality. In total, 380 structures containing at least one R–Y···LB contact belonging to the specific angular range were identified: 162 involving sulfur or tellurium, and 56 involving selenium. The raw data are displayed as bar charts in Fig. S1. The results were grouped in two containers: those in which chalconium cations interact with all bases, and limited to contacts with any anion (see Fig. S1). The data were refined by the standard cone correction[18,97–100] which accounts for the lesser probability that a given point will occur close to the linear 180° position. These corrected probabilities are presented in Fig. 2, which make evident the high propensity toward linearity. The 175–180° slot accounts for more than 40% population for S and Te atoms, slightly less than 40% for Se. Fig. 2, respectively representing cation–neutral and cation–anion pairs. The results of CSD survey make it immediately clear that there is a definite preference for linearity of these chalcogen bonds, whether to any species at all, or to an anion. In the work of Galmes *et al.* seven X-ray structures were found to correspond to the RX_2S pattern (R = any atom, X = halogen).[59]

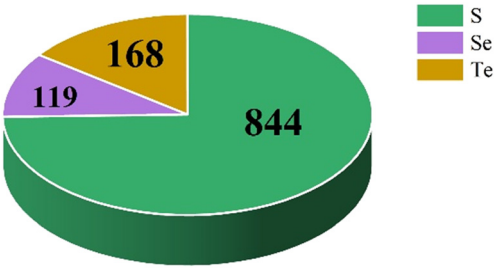

Fig. 1 The pie chart representing distribution of hits in the first stage of the CSD survey.

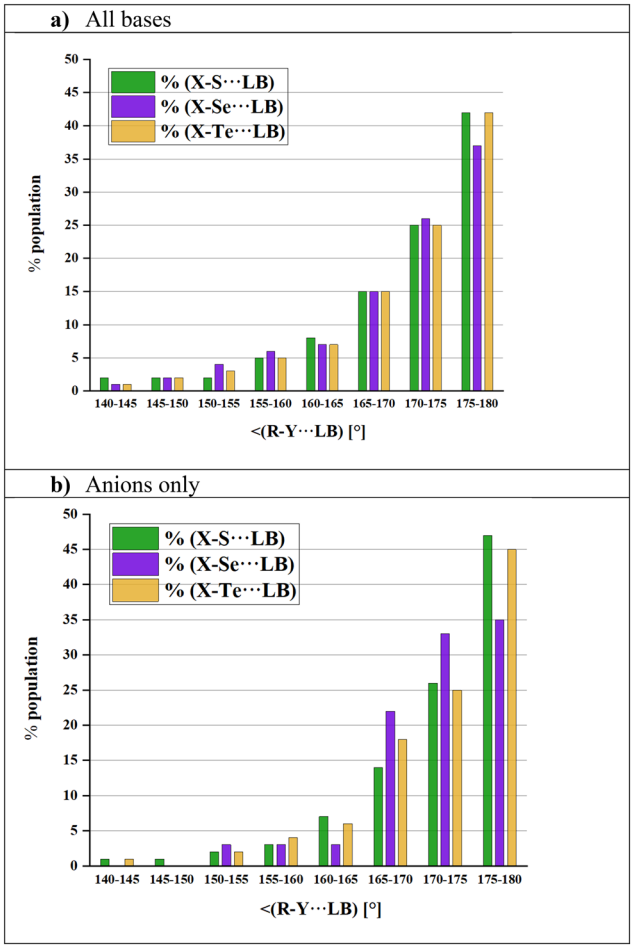

Fig. 2 Bar charts representing the distribution of obtained hits *versus* the R–Y···LB angle after cone correction for the chalconium cation with (a) any base and (b) only anions.

Quantum calculations

To gain more detailed insight into this matter, three sample crystal structures were selected each containing a different chalconium cation $[YR_3]^+$. These structures are displayed in Fig. 3.

In the first one (CSD refcode AMOLUM), two neutral acetonitrile ($NCCH_3$) molecules and one anionic $[SbF_6]^-$ ligand are coordinated to the sulfonium cation $[SF_3]^+$. The S···F–Sb distance is 2.621 Å (compared to a van der Waals radius sum of 3.35 Å), and the F–S···F angle is 172.2°. In the crystal structure with CSD refcode MEKCAI, the central selenonium cation $[Se(CH_3)_3]^+$ is surrounded by three $[TeCl_6]^{2-}$ anions. The Se···Cl distance highlighted in Fig. 3 is 3.377 Å (sum of vdW radius is 3.64 Å), and the C–Se···Cl angle is 168.9°. The most linear geometry is observed for the Te···F interaction in the structure containing telluronium cation, where the mean value of the C–Te···F angle is 173.8°, and the average Te···F distance is 3.089 Å (shorter than the sum of the van der Waals radii by 0.361 Å) (in the case of the latter crystalline solid the angles and distance connected to the cation···anion interactions were inequivalent, therefore

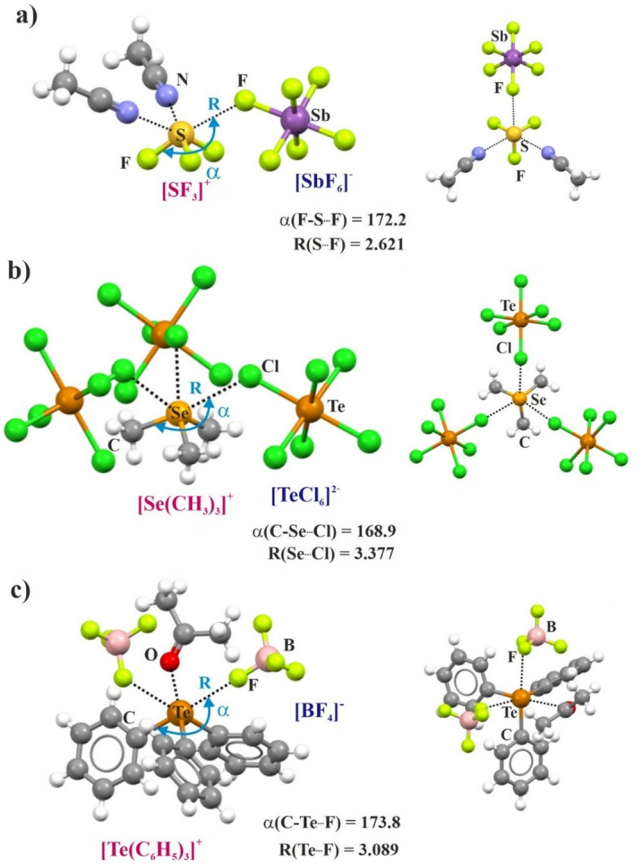

Fig. 3 Fragments of crystal structures featuring chalconium cation···anion motifs: a) $[SF_3]^+\cdots[SbF_6]^-$ (refcode AMOLUM[86]), b) $[Se(CH_3)_3]^+\cdots[TeCl_6]^-$ (refcode MEKCAI[87]), c) $[Te(C_6H_5)_3]^+\cdots[BF_4]^-$ (RILFOL[88]). Each structure is shown in two orientations: side view (left) and top view (right).

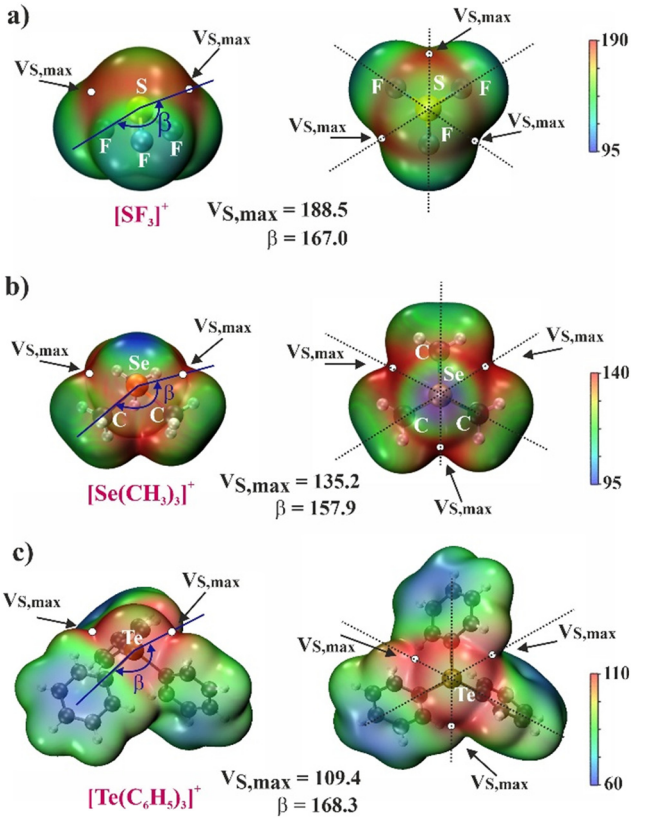

Fig. 4 Molecular electrostatic potential (MEP) surrounding a) $[SF_3]^+$, b) $[Se(CH_3)_3]^+$ and c) $[Te(C_6H_5)_3]^+$ cations in the geometry of corresponding crystal structures. Each MEP is shown in two orientations: side view (left) and top view (right). Dashed lines indicate the directions of S–F, Se–C and Te–C bonds. Small white spots mark the positions of $V_{S,max}$ on the 0.001 a.u. isodensity surface. The numbers on scale as well as average values of $V_{S,max}$ are given in kcal mol^{-1}, averages angles in degrees.

the average values are highlighted in Fig. 3). The overall analysis of interatomic distances revealed that in each case the Y···LB contact was shorter than the sum of van der Waals radii of respective atoms (between 69% and 93%) but at the same time longer than the sum of the corresponding covalent radii (by a factor of 1.5). One can conclude, that the investigated interactions are noncovalent but certainly attractive.

Subsequently, the directionality of the interaction between the anionic ligands and the chalconium cations was examined to determine whether it could be attributed to an unequal distribution of electrostatic potential around the $[YR_3]^+$ (Y = S, Se, Te) cation–analogous to the behavior observed in noncovalent interactions such as hydrogen, halogen, or chalcogen bonds.[73,101] However, it must be noted that in the case of chalconium cations, where a region of high positive electrostatic potential encompasses the entire chalcogen atom, the situation differs from that of archetypal σ-hole donors in neutral Lewis acids, in which the σ-hole is typically surrounded by regions of negative MEP. Therefore, for each of the three systems under consideration, the molecular electrostatic potential around the isolated chalconium cation in its crystal geometry was calculated. For clarity, these distributions are presented in two orientations (see Fig. 4). In addition to the positions of the maxima, the figure also includes straight lines passing through the corresponding covalent bonds, indicated by dashed lines. The average values of the three marked maxima ($V_{S,max}$) and the angles F–Y···$V_{S,max}$ or C–Y···$V_{S,max}$ are also provided. The highest average value of $V_{S,max}$, is 188.5 kcal mol^{-1}, recorded for the $[SF_3]^+$ cation, which is consistent with the literature value of 186.9 kcal mol^{-1}, calculated for this cation at the B3LYP/aug-cc-pVTZ level.[86] For comparison the MEP maxima for $[R_3Ch]^+[BF_4]^-$ salts studied earlier[59] were lower (from 52.7 to 99.8 kcal mol^{-1}) using PBE0-def2TZVP level which was a consequence of defining the investigated monomeric model as the neutral one, contrary to the current work where the monomers are studied as bare cations. The lowest $V_{S,max}$ value, 109.4 kcal mol^{-1} was found for the $[Te(C_6H_5)_3]^+$ cation. Comparing the values of corresponding β angle (Fig. 4) with the value of α angle (Fig. 3), it can be seen that in all three cases, α is closer to 180°. That is, the nucleophilic atom lies some 5–11° closer to the RY bond extension than does the maximum in the MEP. The S···F–

Sb angle is some 133.4° which facilitates the F lone pair alignment with the σ*(FS) antibonding orbital.

The measure of strength of these forces was taken to be the interaction energy. For the purpose of estimating this quantity, the cation···anion dimers were extracted from the crystal structures provided by CSD. Such dimeric constructs do not mimic the entire network of particles contained throughout the crystal structures so represent an approximation involving only these nearest neighbors. The largest absolute value of interaction energy was computed for the $[Se(CH_3)_3]^+\cdots[TeCl_6]^{2-}$ dimer. Three equivalent energies of −134.32 kcal mol^{-1} indicated high stabilization of these compounds driven by the cation···dianion interactions. In two remaining crystals, the cation···monoanion contacts yielded the somewhat smaller interaction energies: −91.90 kcal mol^{-1} for sulfuronium cation···$[SbF_6]^-$, and −76.11 or −69.82 kcal mol^{-1} for telluronium cation···$[BF_4]^-$ dimers. As in the case of MEP maxima, also interaction energies obtained by Galmes *et al.* for chalconium salts paired with neutral tripodal electron donors[59] were considerably smaller (in terms of absolute numbers) due to the presence of neutralized cationic entity and its neutral acceptor. They were in broad range, from −77 to −13 kcal mol^{-1}. In the biologically relevant complex of salacinol (sulfonium cation type) interacting with a model of aspartate the interaction energy was as high as −38.5 kcal mol^{-1}.[59]

In the current work we performed a deeper analysis in order to explain the origin of the anisotropy of the complexes stabilized by charge-assisted chalcogen bond. To this end, we executed the ALMO-EDA decomposition of the interaction energy between two ions depicted in Fig. 5a.

According to the ALMO-EDA, the broken green curve representing the total energy, has its minimum in the vicinity of θ = 10°, *i.e.* 10° from the F–S bond projections, and very close to the crystal value of 8.2°. The position of this minimum results from a compromise between the electrostatic term (ES, black curve) which favors larger θ and the repulsive exchange component (EX, red curve) which stabilizes in the opposite direction, away from the other two F centers of SF_3^+. The other three attractive components (polarization POL, charge transfer CT, and dispersion DISP) are fairly insensitive to θ, so do not exert a major influence upon the optimum angle. A more detailed look at these latter quantities is contained in Fig. 5c. The POL component is the most negative, rather than CT, and dispersion favors larger rather than smaller θ. The latter effect is likely due to the rising dispersive attractions between the F atoms of the two ions. Note that CT is most favorable for very small θ angles, due to the optimum overlap with the FS antibonding orbitals of the cation. Fig. 5d combines the ES and EX terms, the sum of which contains a minimum roughly at the angle observed in the crystal structures. The main conclusion is that the optimum placement of the F atom of the anion is close to the FS bond extension, due to the opposing trends of electrostatic attraction and exchange repulsion. These

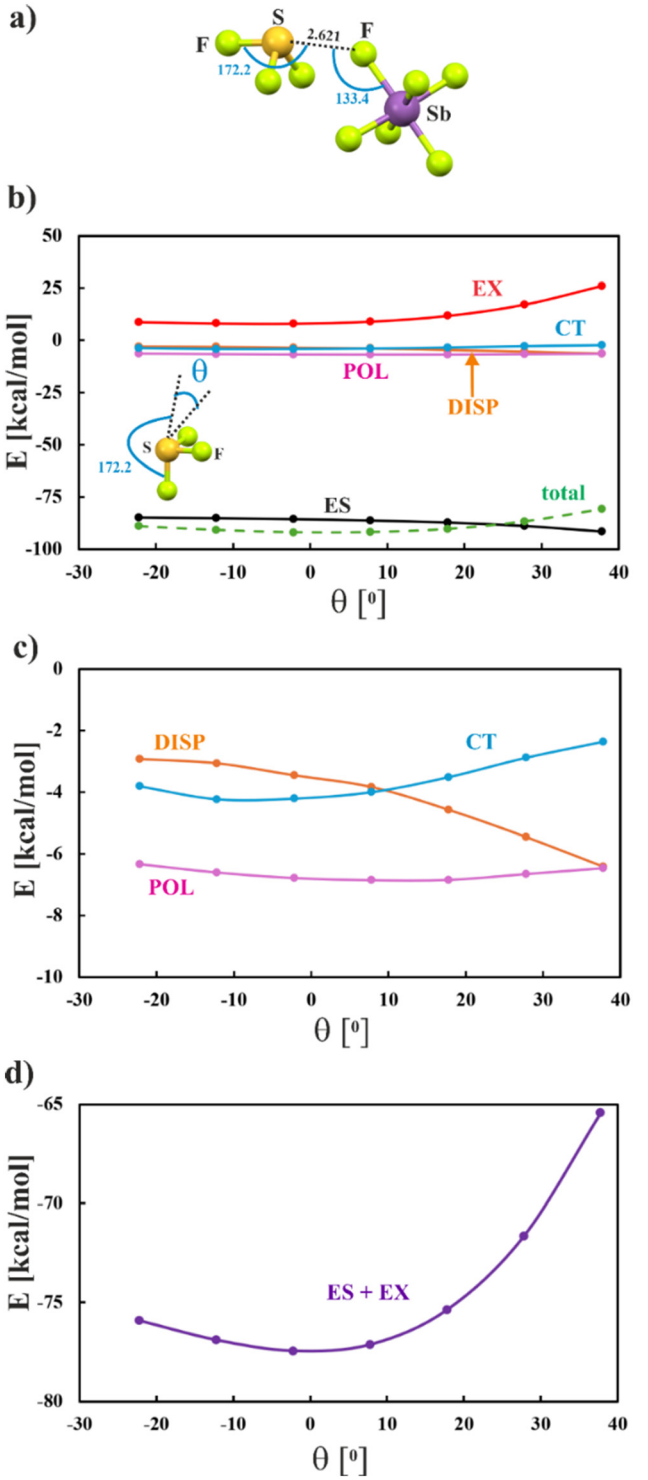

Fig. 5 Geometry of complex pairing SF_3^+ with SbF_6^- a) showing crystal geometrical parameters, b–d) ALMO-EDA components of the interaction energy.

trends remain intact when Se and Te-containing crystals are considered.

In addition to the electrostatic attraction between the SF_3^+ cation and a negative counterion, there ought to be a certain amount of charge transfer from the latter to the former. The

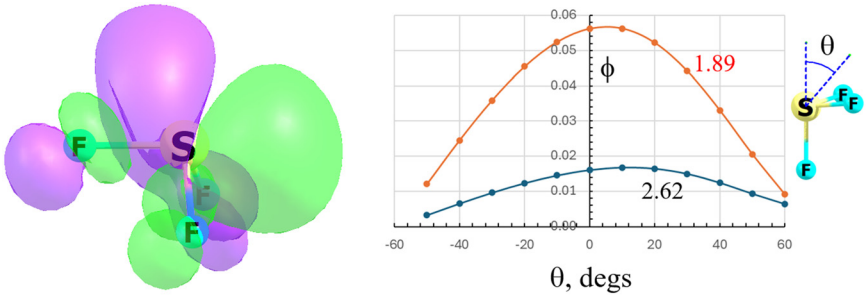

Fig. 6 LUMO + 1 orbital of SF_3^+ spatial disposition where green and purple colors indicate opposite sign of the wavefunction (left) and value of the wavefunction φ at two indicated distances (in Å) from S as a function of θ angle (right).

low-lying orbital of SF_3^+ which is best aligned to receive this charge from an electron donor to its right is the LUMO + 1 whose spatial disposition is illustrated in Fig. 6. Like the density and MEP, the green lobe of this orbital reaches its maximum close to the F–S extension, with θ around 10°, as is evident in the diagram to its right. This shape is basically identical, whether at the vdW radius of 1.89 Å or that pertinent to the counterion F position of R = 2.62 Å.

Discussion

The angular dependence of these cation–anion ion pairs stabilized by the charge-assisted chalcogen bond can be compared to what is observed in neutral systems. Previous calculations of the chalcogen bond within HFS···NH_3 had found a far weaker interaction of about 8 kcal mol^{-1}.[102] This quantity quickly weakened as the orientation was distorted from its near linear preferred configuration. For example, the interaction energy was cut in half by a deformation of about 15°, and was eliminated entirely if the bend rose above about 25°. The contrast with the currently investigated ion pairs is obvious. In the first place these interaction energies exceed 80 kcal mol^{-1}, an order of magnitude larger than in the neutral system. And while there is some loss upon angular distortion of the ion pairs from their optimal alignment, that decrease is far smaller such that these interactions remain highly exothermic over the entire range of angles considered, covering more than 70° in all. On a percentage basis, the neutral HFS···NH_3 loses roughly half of its stability upon a 20° distortion. The same 20° bend results in a reduction of the ion pair interaction energies of only some 1–3%.

On the other hand, one should not entirely lose sight of the directionality of these ion pair bonds as the energy does indeed change as nonlinearity is introduced. An alternate view of this property derives from the curvature of the energy *versus* the θ angle. These two quantities can be conveniently fit to a harmonic expression: $E = \frac{1}{2}k\theta^2$, where k represents a bending force constant. For the three charged systems discussed above, this force constant varies between 30 and 70 kcal mol^{-1} rad^2. To place these values in perspective, they are larger than k for the neutral pair chalcogen bonds studied earlier,[102] that varied between 3.4 and 7.9 kcal mol^{-1} rad^2. So in this frame of reference, the directionality of chalcogen bonds remains when the neutral pairs are mutated to ion pairs.

In a sense then, some precision and context is needed in any discussion of directionality. Neutral and ion pairs are different at some fundamental levels. The latter is far stronger than the former. As a consequence, even if a given nonlinear distortion imposed on an ion pair results in a similar loss in stability as in a neutral pair, the percentage reduction of the interaction energy will be far smaller in the ion pair. Secondly, only relatively small deformations can cause the interaction to turn from attractive to repulsive in a neutral pair. The much deeper potential well in the ion pair case allows the interaction to remain attractive even for high degrees of angular deformation.

The earlier study of neutral dimers had pinpointed exchange repulsion as the chief source of the loss of stability as the chalcogen bond was bent. Taking HFS···NH_3 as the prototype, a 30° deformation caused the exchange repulsion to rise by 5.6 kcal mol^{-1}, much larger than the 1 kcal mol^{-1} destabilization of the electrostatic and induction energies. This distinction is even more dramatic for ClFS···NH_3 or CF_3-HS···NH_3 where the exchange term is the only one that is destabilized by the imposed nonlinearity. These results comport reasonably well with the trends visualized for the ion pairs in the current work, where EX is frequently at odds with ES but it is the former whose changes are larger in magnitude.

In a broader sense, the dominating influence of electrostatics and exchange repulsion in controlling the angular preferences of these ion pairs is consistent with neutral pairs, not only of chalcogen bond types. Exchange repulsion in particular has been shown to be a dominating factor in hydrogen, halogen, and pnicogen bonds as well.[102–107] The extraordinarily large attractive coulombic forces within ion pairs magnifies the electrostatic component, such that it grows to play a role that is competitive with exchange repulsion.

The calculated results presented above provide a framework to explain the trend toward linearity of chalcogen bonds, of both neutral and ion pair types. At the same time, one should remember that the very high attractive forces present within the ion pairs will retain a high interaction energy even in the face of significant nonlinearities. The

preference of a fluoride anion for the σ-hole positions of a chalcogen atom within a cation is consistent with some very recent calculations involving benzimidazoliums.[108] There have been some earlier studies that considered the directionality of salts containing halogen bonds between ions. But in some cases, the directionality of the halogen bond seemed to be an indirect result of the H-bonds that were also present and dominated the intermolecular orientations.[109] It is finally noted that the directionality of the ion-pair charge-assisted chalcogen bonds discussed here is an intrinsic property of these systems, and is not attributable to the flanking of the active section of the cation by inert hydrophobic groups that restrict the access of the anionic Lewis base, as proposed recently.[33]

Conclusions

In summary, an inspection of the Cambridge Structural Database exhibited linear chalcogen bonds between chalconium cations $[R_3Y]^+$ (Y = S, Se, Te) and various anions. Among 380 X-ray structures containing such cation···anion contacts, after cone correction, nearly half of the sulfur-based interactions fall within the 175–180° range of the $[R_3Y]^+$···anion angle, followed by 45% for tellurium and 35% for selenium. These results demonstrate that these strong charge-assisted chalcogen bonds exhibit pronounced directionality. Quantum chemical analysis traces this linearity to a compromise between two factors, electrostatic attraction and exchange repulsion which pull in opposite directions. Because of the strong attraction between ions of opposite charge, the interaction energy remains highly negative, even for large distortions from linearity. The importance of exchange repulsion to the angular aspects is consistent with similar findings in neutral chalcogen and other noncovalent bonds.

Conflicts of interest

There are no conflicts to declare.

Data availability

The data supporting this article have been included as part of the supplementary information (SI).

Supplementary information: Fig. S1: bar charts representing the distribution of obtained hits *versus* the R–Y···LB angle prior to cone correction for all contacts to chalconium cations; Table S1: coordinates of investigated structures. See DOI: https://doi.org/10.1039/d6ce00102e.

Acknowledgements

The authors (M. M. and W. Z.) gratefully acknowledge Wrocław Center for Networking and Supercomputing (WCSS). This work was financed *via* the grant "MINIATURA" from National Science Centre (Poland) awarded to M. M., the grant number 2025/09/X/ST4/00174. This material is also based upon work supported by the U.S. National Science Foundation under Grant No. 1954310 to S. S. This work was financed in part by a statutory activity subsidy from the Polish Ministry of Science and Higher Education for the Faculty of Chemistry of Wroclaw University of Science and Technology.

References

1 G. R. Desiraju and T. Steiner, *The Weak Hydrogen Bond: In Structural Chemistry and Biology*, Oxford University Press, New York, 1999.
2 N. Xu, J. Han, Z. G. Zhu, B. Song, X. H. Lu and Y. L. Cai, *Soft Matter*, 2015, **11**, 5546–5553.
3 F. Haso, J. C. Luo, B. S. Bassil, B. Artetxe, J. Zhou, P. C. Yin, S. Reinoso, J. M. Gutierrez-Zorrilla, U. Kortz and T. B. Liu, *ChemistrySelect*, 2016, **1**, 4345–4349.
4 H. T. Huynh, O. Jeannin and M. Fourmigué, *Chem. Commun.*, 2017, **53**, 8467–8469.
5 X. Bin, T. Xu, S. R. Kirk and S. Jenkins, *Chem. Phys. Lett.*, 2019, **730**, 506–512.
6 J. Wang, G. Lu, Y. Liu, S. G. Wu, G. Z. Huang, J. L. Liu and M. L. Tong, *Cryst. Growth Des.*, 2019, **19**, 1896–1902.
7 M. M. Zhai, Q. Chen, W. Yuan, Q. X. Shi and H. Xu, *Mater. Chem. Front.*, 2019, **3**, 1888–1891.
8 A. Martínez-Camarena, M. Savastano, J. M. Llinares, B. Verdejo, A. Bianchi, E. García-España and C. Bazzicalupi, *Inorg. Chem. Front.*, 2020, **7**, 4239–4255.
9 A. Dhaka, O. Jeannin, E. Aubert, E. Espinosa and M. Fourmigué, *Chem. Commun.*, 2021, **57**, 4560–4563.
10 N. P. Martin and M. Nyman, *Angew. Chem., Int. Ed.*, 2021, **60**, 954–960.
11 E. G. Noya, C. K. Wong, P. Llombart and J. P. K. Doye, *Nature*, 2021, **596**, 367.
12 J. Vainauskas, T. H. Borchers, M. Arhangelskis, L. J. M. McPherson, T. S. Spilfogel, E. Hamzehpoor, F. Topic, S. J. Coles, D. F. Perepichka, C. J. Barrett and T. Friscic, *Chem. Sci.*, 2023, **14**, 13031–13041.
13 X. F. Wang, Y. L. Hu, L. M. Li, R. Ju, X. F. Han, H. H. Tan, X. X. Ruan, R. Lei, N. Wang, J. Y. Wang and X. Y. Wang, *ACS Appl. Nano Mater.*, 2023, **6**, 7310–7322.
14 S. G. Xu, X. T. Li, Z. J. Chen, C. C. He, C. He, X. B. Yang and H. Xu, *Phys. Rev. Mater.*, 2023, **7**, 084202.
15 Y. Chen, D. Karolly, A. Kuvayskaya, M. Pink, V. Carta, A. Sellinger and A. H. Flood, *Chem*, 2024, **10**, 3582–3594.
16 A. A. Kuznetsova, V. V. Yanshole, M. V. Il'in, A. S. Novikov, D. S. Bolotin, M. N. Sokolov and P. A. Abramov, *Inorg. Chem. Front.*, 2024, **11**, 8902–8915.
17 M. O'Shaughnessy, J. Glover, R. Hafizi, M. Barhi, R. Clowes, S. Y. Chong, S. P. Argent, G. M. Day and A. I. Cooper, *Nature*, 2024, **630**, 102–108.
18 V. R. Boro, B. K. Saha and G. Rangazhvar, *Chem. Commun.*, 2025, **61**, 945–948.
19 E. Kaitatzi, L. Fritsche and S. Kubik, *Chemistry*, 2025, **4**, 129.
20 R. Y. Lu, N. N. Du, S. J. Jiang, M. Lu and P. C. Wang, *Cryst. Growth Des.*, 2025, **25**, 4304–4315.
21 D. Y. Zhang, R. L. Snider, M. R. Crawley and T. R. Cook, *J. Coord. Chem.*, 2025, **78**, 2081–2093.

22 J. S. Murray, K. E. Riley, P. Politzer and T. Clark, *Aust. J. Chem.*, 2010, **63**, 1598–1607.
23 P. Politzer, J. S. Murray and T. Clark, *Phys. Chem. Chem. Phys.*, 2010, **12**, 7748–7757.
24 Z. P. Shields, J. S. Murray and P. Politzer, *Int. J. Quantum Chem.*, 2010, **110**, 2823–2832.
25 J. S. Murray, G. Resnati and P. Politzer, *Faraday Discuss.*, 2017, **203**, 113–130.
26 P. Politzer and J. S. Murray, *Crystals*, 2018, **8**, 42.
27 J. F. Liebman, M. J. Romm, M. Meot-Ner, S. M. Cybulski and S. Scheiner, *J. Phys. Chem.*, 1991, **95**, 1112–1119.
28 M. Meot-Ner, L. W. Sieck, J. F. Liebman and S. Scheiner, *J. Am. Chem. Soc.*, 1996, **100**, 6445–6450.
29 J. F. Liebman and S. Scheiner, *Struct. Chem.*, 1999, **10**, 391–392.
30 M. Meot-Ner, S. M. Cybulski, S. Scheiner and J. F. Liebman, *J. Phys. Chem.*, 1988, **92**, 2738–2745.
31 R. F. W. Bader and W. H. Henneker, *J. Am. Chem. Soc.*, 1965, **87**, 3063.
32 F. Illas, A. Lorda, J. Rubio, J. B. Torrance and P. S. Bagus, *J. Chem. Phys.*, 1993, **99**, 389–396.
33 I. Hutskalov, A. Linden and I. Coric, *J. Am. Chem. Soc.*, 2023, **145**, 8291–8298.
34 K. R. Kong, J. Wang, P. L. Zhang, X. M. Ma, Y. F. Xu, Z. Q. Ma, Y. H. Sang, Z. S. Zhang, T. R. Liu, C. H. Jin, Z. M. Liu and R. K. Tang, *J. Phys. Chem. Lett.*, 2024, **15**, 2624–2631.
35 A. A. Ganie, A. A. Ahangar and A. A. Dar, *Cryst. Growth Des.*, 2019, **19**, 4650–4660.
36 N. G. White, *Dalton Trans.*, 2019, **48**, 7062–7068.
37 G. K. H. Shimizu, R. Vaidhyanathan and J. M. Taylor, *Chem. Soc. Rev.*, 2009, **38**, 1430–1449.
38 Y. Haketa and H. Maeda, *Chem. Commun.*, 2017, **53**, 2894–2909.
39 O. Nordness and J. F. Brennecke, *Chem. Rev.*, 2020, **120**, 12873–12902.
40 K. Fumino and R. Ludwig, *J. Mol. Liq.*, 2014, **192**, 94–102.
41 S. Tsuzuki, H. Tokuda, K. Hayamizu and M. Watanabe, *J. Phys. Chem. B*, 2005, **109**, 16474–16481.
42 C. J. Rogers, S. Koutsoukos, J. Eisermann, L. Wylie, G. J. Smith, T. Welton and M. M. Roessler, *Angew. Chem., Int. Ed.*, 2025, **64**, e202504882.
43 A. Grabarz, M. Michalczyk, W. Zierkiewicz and S. Scheiner, *Molecules*, 2021, **26**, 2116.
44 M. Michalczyk, W. Zierkiewicz, R. Wysokinski and S. Scheiner, *Phys. Chem. Chem. Phys.*, 2021, **23**, 25097–25106.
45 R. Wysokinski, M. Michalczyk, W. Zierkiewicz and S. Scheiner, *Phys. Chem. Chem. Phys.*, 2021, **23**, 4818–4828.
46 R. Wysokinski, W. Zierkiewicz, M. Michalczyk and S. Scheiner, *ChemPhysChem*, 2021, **22**, 818–821.
47 I. Mata, E. Molins, I. Alkorta and E. Espinosa, *J. Phys. Chem. A*, 2015, **119**, 183–194.
48 M. O. Miranda, D. J. R. Duarte and I. Alkorta, *ChemPhysChem*, 2020, **21**, 1052–1059.
49 D. Quiñonero, I. Alkorta and J. Elguero, *ChemPhysChem*, 2020, **14**, 1597–1607.
50 V. A. Aliyeva, V. André, L. M. D. R. S. Martins, A. Frontera and K. T. Mahmudov, *Coord. Chem. Rev.*, 2026, **549**, 217257.
51 E. Bartashevich, S. Mukhitdinova, I. Yushina and V. Tsirelson, *Acta Crystallogr., Sect. B: Struct. Sci., Cryst. Eng. Mater.*, 2019, **75**, 117–126.
52 L. Brammer, *Faraday Discuss.*, 2017, **203**, 485–507.
53 W. H. Cai, Z. Y. Li, W. C. Zhou, H. L. Chen, Y. E. Xu, Q. H. Zhu and Y. Zou, *J. Chem. Inf. Model.*, 2025, **65**, 9610–9622.
54 E. V. Ignatov, L. E. Zelenkov, S. V. Baykov, S. Burguera, A. Frontera, N. A. Bokach and V. Y. Kukushkin, *J. Phys. Chem. A*, 2025, **129**, 10661–10672.
55 J. Q. Liu, Y. Zhang and W. Z. Wang, *J. Phys. Chem. A*, 2025, **129**, 7670–7678.
56 A. Pizzi, G. Terraneo, C. Lo Iacono, R. Beccaria, A. Dhaka and G. Resnati, *Angew. Chem., Int. Ed.*, 2025, **64**, e202506525.
57 A. Tripathi, M. Calabrese, A. Pizzi, A. Dhaka, N. Demitri, D. R. Turner, G. B. Deacon, A. Frontera, G. Resnati and H. B. Singh, *Chem. – Asian J.*, 2025, **20**, e202401846.
58 H. Y. Zhou, X. Wang, X. L. An, Q. Z. Li and S. A. C. McDowell, *CrystEngComm*, 2025, **27**, 4516–4527.
59 B. Galmes, A. Juan-Bals, A. Frontera and G. Resnati, *Chemistry*, 2020, **26**, 4599–4606.
60 M. d. l. N. Piña, A. Frontera and A. Bauza, *ACS Chem. Biol.*, 2021, **16**, 1701–1708.
61 L. M. Lee, V. Corless, H. Luu, A. He, H. Jenkins, J. F. Britten, F. Adam Pani and I. Vargas-Baca, *Dalton Trans.*, 2019, **48**, 12541–12548.
62 J. Y. C. Lim, I. Marques, A. L. Thompson, K. E. Christensen, V. Félix and P. D. Beer, *J. Am. Chem. Soc.*, 2017, **139**, 3122–3133.
63 S. Ghinato, A. Giordana, E. Diana, R. M. Gomila, E. Priola and A. Frontera, *Dalton Trans.*, 2023, **52**, 15688–15696.
64 A. Zabardasti, Z. M. Abd Al-Aama, N. J. Hussein, M. N. Al-Baiati and M. Salehnassaj, *J. Sulfur Chem.*, 2025, **46**, 1210–1224.
65 T.-N. Streit, R. M. Gomila, R. Sievers, A. Frontera and M. Malischewski, *CrystEngComm*, 2024, **26**, 594–598.
66 R. J. Fick, G. M. Kroner, B. Nepal, R. Magnani, S. Horowitz, R. L. Houtz, S. Scheiner and R. C. Trievel, *ACS Chem. Biol.*, 2016, **11**, 748–754.
67 G. Feng, G. Wei, J. Luo, D. Zhang, L. Hou, M. Xing, R. Guo, S. Xu, Y. Luo, G. Yang and Y. Zhang, *Int. J. Pharm.*, 2025, **686**, 126355.
68 S. Zuo, T. Liu, L. Li, H. Xu, J. Guo, Q. Wang, Y. Yang, Z. He, J. Sun and B. Sun, *Cell Rep. Med.*, 2024, **5**, 101432.
69 M. Ochiai, T. Suefuji, K. Miyamoto, N. Tada, S. Goto, M. Shiro, S. Sakamoto and K. Yamaguchi, *J. Am. Chem. Soc.*, 2003, **125**, 769–773.
70 A. S. Novikov and D. S. Bolotin, *Org. Biomol. Chem.*, 2022, **20**, 7632–7639.
71 A. A. Sysoeva, Y. V. Safinskaya, M. V. Il'in, A. S. Novikov and D. S. Bolotin, *Org. Biomol. Chem.*, 2025, **23**, 1970–1980.
72 P. Politzer, J. S. Murray, T. Clark and G. Resnati, *Phys. Chem. Chem. Phys.*, 2017, **19**, 32166–32178.
73 P. Politzer and J. S. Murray, *Crystals*, 2017, **7**, 212.
74 J. S. Murray and P. Politzer, *J. Mol. Model.*, 2019, **25**, 101.

75 J. S. Murray, P. Lane and P. Politzer, *J. Mol. Model.*, 2009, **15**, 723–729.
76 J. S. Murray and P. Politzer, *WIREs Comput. Mol. Sci.*, 2011, **1**, 153–163.
77 P. Politzer, J. S. Murray and T. Clark, *Top. Curr. Chem.*, 2015, **358**, 19–42.
78 M. Michalczyk, *ChemPhysChem*, 2025, 2500357.
79 I. O. Putnin, A. A. Sysoeva, A. V. Kovalenko and D. S. Bolotin, *Org. Biomol. Chem.*, 2025, **23**, 7197–7205.
80 L. Turunen and M. Erdélyi, *Chem. Soc. Rev.*, 2020, **49**, 2688–2700.
81 F. Weigend, *Phys. Chem. Chem. Phys.*, 2006, **8**, 1057–1065.
82 F. Weigend and R. Ahlrichs, *Phys. Chem. Chem. Phys.*, 2005, **7**, 3297–3305.
83 Y. Zhao and D. G. Truhlar, *Acc. Chem. Res.*, 2008, **41**, 157–167.
84 Y. Zhao and D. G. Truhlar, *Theor. Chem. Acc.*, 2008, **120**, 215–241.
85 M. J. Frisch, G. W. Trucks, H. B. Schlegel, G. E. Scuseria, M. A. Robb, J. R. Cheeseman, G. Scalmani, V. Barone, G. A. Petersson, H. Nakatsuji, X. Li, M. Caricato, A. V. Marenich, J. Bloino, B. G. Janesko, R. Gomperts, B. Mennucci, H. P. Hratchian, J. V. Ortiz, A. F. Izmaylov, J. L. Sonnenberg, F. Williams, F. Ding, F. Lipparini, F. Egidi, J. Goings, B. Peng, A. Petrone, T. Henderson, D. Ranasinghe, V. G. Zakrzewski, J. Gao, N. Rega, G. Zheng, W. Liang, M. Hada, M. Ehara, K. Toyota, R. Fukuda, J. Hasegawa, M. Ishida, T. Nakajima, Y. Honda, O. Kitao, H. Nakai, T. Vreven, K. Throssell, J. A. Montgomery Jr., J. E. Peralta, F. Ogliaro, M. J. Bearpark, J. J. Heyd, E. N. Brothers, K. N. Kudin, V. N. Staroverov, T. A. Keith, R. Kobayashi, J. Normand, K. Raghavachari, A. P. Rendell, J. C. Burant, S. S. Iyengar, J. Tomasi, M. Cossi, J. M. Millam, M. Klene, C. Adamo, R. Cammi, J. W. Ochterski, R. L. Martin, K. Morokuma, O. Farkas, J. B. Foresman and D. J. Fox, *Gaussian 16 Rev. C.01*, Wallingford, CT, 2016.
86 D. Turnbull, P. Chaudhary, P. Hazendonk, S. D. Wetmore and M. Gerken, *Inorg. Chem.*, 2021, **60**, 3893–3901.
87 A. L. Hector, A. Jolleys, W. Levason and G. Reid, *Dalton Trans.*, 2012, **41**, 10988–10999.
88 L. Groslambert, A. Padilla-Hernandez, R. Weiss, P. Pale and V. Mamane, *Chem. – Eur. J.*, 2023, **29**, e202203372.
89 C. R. Groom, I. J. Bruno, M. P. Lightfoot and S. C. Ward, *Acta Crystallogr., Sect. B: Struct. Sci., Cryst. Eng. Mater.*, 2016, **72**, 171–179.
90 T. Lu and F. Chen, *J. Mol. Graphics Modell.*, 2012, **38**, 314–323.
91 T. Lu and F. Chen, *J. Comput. Chem.*, 2012, **33**, 580–592.
92 W. Humphrey, A. Dalke and K. Schulten, *J. Mol. Graphics Modell.*, 1996, **14**, 33–38.
93 S. F. Boys and F. Bernardi, *Mol. Phys.*, 1970, **19**, 553–566.
94 P. R. Horn, Y. Mao and M. Head-Gordon, *Phys. Chem. Chem. Phys.*, 2016, **18**, 23067–23079.
95 P. R. Horn, Y. Mao and M. Head-Gordon, *J. Chem. Phys.*, 2016, **144**, 114107.
96 G. A. Zhurko, *Chemcraft*.
97 L. Brammer, E. A. Bruton and P. Sherwood, *Cryst. Growth Des.*, 2001, **1**, 277–290.
98 J. Kroon and J. A. Kanters, *Nature*, 1974, **248**, 667–669.
99 A. Saha, S. A. Rather, D. Sharada and B. K. Saha, *Cryst. Growth Des.*, 2018, **18**, 6084–6090.
100 J. A. van den Berg and K. R. Seddon, *Cryst. Growth Des.*, 2003, **3**, 643–661.
101 J. S. Murray and P. Politzer, *WIREs Comput. Mol. Sci.*, 2017, **7**, e13260.
102 U. Adhikari and S. Scheiner, *Chem. Phys. Lett.*, 2012, **532**, 31–35.
103 G. Haberhauer and R. Gleiter, *Angew. Chem., Int. Ed.*, 2020, **59**, 21236–21243.
104 K. E. Riley, *Chem. Phys. Lett.*, 2020, **744**, 137221.
105 K. E. Riley, M. Vazquez, C. Umemura, C. Miller and K. A. Tran, *Chem. – Eur. J.*, 2016, **22**, 17690–17695.
106 A. J. Stone, *J. Am. Chem. Soc.*, 2013, **135**, 7005–7009.
107 M. M. Szczęśniak and G. Chałasinski, *Front. Chem.*, 2022, **10**, 858946.
108 T. Arndt, M. Partzsch, T. Rüffer and M. Breugst, *Org. Biomol. Chem.*, 2025, **23**, 10574–10585.
109 M. Culig, V. Nemec, N. Bregovic and D. Cincic, *CrystEngComm*, 2025, **47**, 7638–7643.